

Article

Dual-Modal Hybrid Control for an Upper-Limb Rehabilitation Robot

Guang Feng^{1,2,3}, Jiaji Zhang^{2,3,*} , Guokun Zuo^{2,3,*} , Maoqin Li^{2,3}, Dexin Jiang^{1,2,3} and Lei Yang¹

¹ School of Mechatronic Engineering and Automation, Shanghai University, Shanghai 200444, China; fengguang@nimte.ac.cn (G.F.); jiangdexin@nimte.ac.cn (D.J.); yanglei130@shu.edu.cn (L.Y.)

² Ningbo Cixi Institute of BioMedical Engineering, Ningbo Institute of Materials Technology and Engineering, Chinese Academy of Sciences, Cixi 315300, China; limaoqin@nimte.ac.cn

³ Ningbo Institute of Materials Technology and Engineering, Chinese Academy of Sciences, Ningbo 315201, China

* Correspondence: zhangjiaji@nimte.ac.cn (J.Z.); moonstone@nimte.ac.cn (G.Z.)

Abstract: The recovery treatment of motor dysfunction plays a crucial role in rehabilitation therapy. Rehabilitation robots are partially or fully replacing therapists in assisting patients in exercise by advantage of robot technologies. However, the rehabilitation training system is not yet intelligent enough to provide suitable exercise modes based on the exercise intentions of patients with different motor abilities. In this paper, a dual-modal hybrid self-switching control strategy (DHSS) is proposed to automatically determine the exercise mode of patients, i.e., passive and assistive exercise mode. In this strategy, the potential field method and the ADRC position control are employed to plan trajectories and assist patients' training. Dual-modal self-switching rules based on the motor and impulse information of patients are presented to identify patients' motor abilities. Finally, the DHSS assisted five subjects in performing the training with an average deviation error of less than 2 mm in both exercise modes. The experimental results demonstrate that the muscle activation of the subjects differed significantly in different modes. It also verifies that DHSS is reasonable and effective, which helps patients to train independently without therapists.



Citation: Feng, G.; Zhang, J.; Zuo, G.; Li, M.; Jiang, D.; Yang, L. Dual-Modal Hybrid Control for an Upper-Limb Rehabilitation Robot. *Machines* **2022**, *10*, 324. <https://doi.org/10.3390/machines10050324>

Academic Editor: Davide Astolfi

Received: 21 March 2022

Accepted: 20 April 2022

Published: 29 April 2022

Publisher's Note: MDPI stays neutral with regard to jurisdictional claims in published maps and institutional affiliations.



Copyright: © 2022 by the authors. Licensee MDPI, Basel, Switzerland. This article is an open access article distributed under the terms and conditions of the Creative Commons Attribution (CC BY) license (<https://creativecommons.org/licenses/by/4.0/>).

Keywords: rehabilitation robot; potential field; dual-modal switching; human-robot interaction

1. Introduction

Rehabilitation is essential for people with impaired motor function due to age-associated diseases or accidents, in order to fully or partially restore the motor function of their limbs [1]. Due to the shortage of therapists and the cost of various rehabilitation expenses, a great deal of research has been conducted on robot-assisted rehabilitation. Researchers have applied robotics to the field of upper limb rehabilitation and have developed a variety of devices. Examples include end-traction devices: MIT-MANUS [2], MIME [3], EULRR [4], and BULReD [5]; and exoskeletal rehabilitation devices: ARMin [6] and UL-EXO7 [7–9]. These rehabilitation robots can provide multiple modes of rehabilitation exercises: passive exercise, assistive exercise, and resistance exercise.

The human–robot interaction control strategy of the rehabilitation robots is also a key factor affecting the rehabilitation results. The patient's initial rehabilitation focuses on unidirectional master–slave passive exercise; and upper limb rehabilitation robots generally use position control strategies such as classical PID control, sliding mode control [10], and active disturbance rejection control (ADRC) [11]. In addition, passive exercise puts high demands on precision and safe motion planning. Thus, a motion planning strategy with minimal potential energy modulation has been proposed [12]. However, passive exercise strictly follows the physician's pre-defined trajectory without any form of interaction between patients and rehabilitation robots during the whole training process [13]. Patients will eventually lose active participation in passive exercise. Research findings [14] in

sports rehabilitation medicine have shown that active participation in training has a crucial impact on the recovery of motor learning ability and on the improvement of rehabilitation outcomes, because some patients with severe motor impairment can produce muscle activity but not movement or strength. Some studies [15–17] have used EMG-triggered control strategies to assist training.

The control methods for assistive exercise are more diverse. Assist-as-needed (AAN) control strategies [18–20] are often applied in assistive exercise mode. AAN control strategies firstly develop rules to assess the patient's motor ability and secondly generate different assistive forces based on the patient's motor status. However, changes in tracking error-based assisted force inevitably lead to negative training. Study [21] has also proposed a reward–punishment feedback control strategy. It provides rewarding feedback or punishing feedback when patient training participation is high or low, respectively, which helps to avoid patient slacking. Some preliminary studies that are more directly related to the present study should be cited: [22,23]. Study [22] has proposed a time-invariant control strategy: unified motion and variable impedance control (UMIC). By building the potential and dissipative fields, the motion of the industrial robotic arm on the desired trajectory is controlled. Literature [23] further proposes a rehabilitation training control strategy based on potential and velocity fields using the UMIC. UMIC does not assist training based on tracking errors, but provides control quantities based on a pre-designed potential field model.

The essence of the human–robot interaction control strategy is to adjust both the intensity of the rehabilitation robot's assistance as well as the mode according to the patient's motor intention, to encourage active participation in the training. A large number of studies have used sEMG to identify patients' motor intentions and to assess their motor function. Offline upper limb sEMG signals are used to identify functional movements and assess the level of limb impairment of patients with stroke [24–26]. Literature [27] proposes an SVM classifier-based sEMG to determine movements of healthy side limb, and to replicate the movements in the affected side limb for training. However, due to the variability of the human body, it is still quite difficult to accurately predict the motor intention of patients online based on sEMG.

The assistance torque required by patients is different at different stages of rehabilitation and motor status. It is important to motivate patients by providing assistance torque according to patients' motor intention and motor ability. Study [28] has developed a complete rehabilitation system that can model all the therapeutic exercises for an upper limb rehabilitation, by modifying the control parameters. However, how to switch intelligently between the various exercise modes according to the actual motor ability of patients has not been investigated. This is crucial for rehabilitation devices that are far from or lacking therapists.

In a previous work [29], a robot platform was introduced and an AAN control strategy for bilateral training was proposed. The contribution of this study is the design of a dual-modal hybrid self-switching (DHSS) control strategy that can perform both passive and assistive exercises. This strategy combines the high accuracy of position control with the flexibility of potential field. In addition, another contribution is the proposal of a portable method for assessing patients' motor ability and the design of dual-modal self-switching rules.

2. Materials and Methods

2.1. Upper Limb Rehabilitation Robot

An upper limb rehabilitation robot prototype was developed [29]. The rehabilitation robot described below is designed for patients who have a functional (PFL) and an impaired limb (PIL). The upper limb bilateral rehabilitation robot consists of two robotic arms, one of which is called the affected side manipulator (ASM). The ASM is equipped with three motors (Kollmorgen RGM14A/RGM17A) and a force sensor (ZIm 1826) to assist in the rehabilitation training of the PIL. The motor contains an angle encoder. The ASM contains

three degrees of freedom. The robotic arms can move in a three-dimensional workspace. A schematic diagram of the upper limb bilateral rehabilitation robot is shown in Figure 1. The ASM with three joints is the control object in this paper.

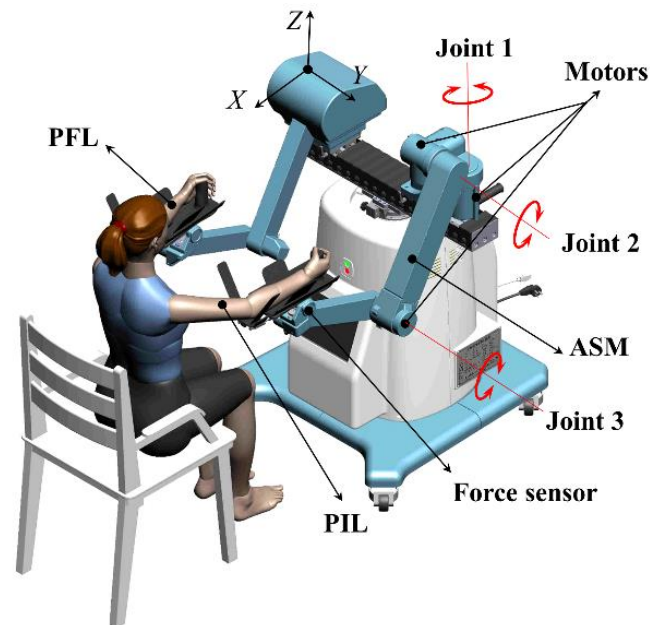


Figure 1. Schematic diagram of upper limb bilateral rehabilitation robot. ASM (the affected side manipulator) is used to assist patients to complete rehabilitation training tasks in a three-dimensional workspace.

The dynamics equation of ASM in joint space are described as follows:

$$M(q)\ddot{q} + C(q, \dot{q})\dot{q} + G(q) + f(\dot{q}) + D = \tau \quad (1)$$

where $q = [\theta_1, \theta_2, \theta_3]$ are the joint angles, $M(q) \in R^{3 \times 3}$ denotes the inertia matrix, $C(q, \dot{q}) \in R^{3 \times 3}$ denotes the Coriolis and centrifugal terms, $G(q) \in R^3$ is the gravity matrix, $f(\dot{q}) \in R^3$ is the friction force, $\tau \in R^3$ denotes the vector of applied torques by actuators, D is the unmodeled dynamic term as well as external disturbances. This paper uses the Lagrange method to obtain the matrices M , C , and G . The Stribeck friction torque model [30] is used to identify the friction term $f(\dot{q})$.

The upper limb rehabilitation robot control system is a multiple input multiple output (MIMO) system. To facilitate the use of ADRC to control the joints of the upper limb rehabilitation robot, this section decouples the robot dynamics model and converts it into a single input single output (SISO) system. Rewrite Equation (1) as:

$$\ddot{q} = M^{-1}\tau - M^{-1}(C\dot{q} + G + f + D) \quad (2)$$

Further simplification:

$$\ddot{q} = A_1 + A_2 + u \quad (3)$$

$$\begin{aligned} A_1 &= -M^{-1}(C\dot{q} + G + f) \\ A_2 &= -M^{-1}D \\ u &= M^{-1}\tau \end{aligned} \quad (4)$$

A_1 is the vector obtained by combining the inertial, friction, and gravity terms. A_2 is the uncertain dynamical model of the system and external disturbances, which are more difficult to measure. The virtual torque u is introduced, so that robot dynamics is decoupled into three independent SISO systems:

$$\begin{bmatrix} \ddot{\theta}_1 \\ \ddot{\theta}_2 \\ \ddot{\theta}_3 \end{bmatrix} = \begin{bmatrix} a_{11} \\ a_{12} \\ a_{13} \end{bmatrix} + \begin{bmatrix} a_{21} \\ a_{22} \\ a_{23} \end{bmatrix} + \begin{bmatrix} u_1 \\ u_2 \\ u_3 \end{bmatrix} \tag{5}$$

When the virtual torque u is known, the actual joint torque τ can be obtained:

$$\tau = Mu \tag{6}$$

2.2. Overall Design of Control Strategy

In this paper, a strategy of hybrid control, ADRC combined potential field, is employed to determine suitable assisted torque for the upper limb rehabilitation robot according to the different motor function characteristics of the patient.

In the passive exercise mode, since the patients lack sufficient motor capacity, the auxiliary torque needs to maintain a high level when the rehabilitation robot drives the patient to track the desired trajectory prescribed by the rehabilitation therapist. To achieve high-precision trajectory tracking in passive exercise mode, the ADRC position control strategy is used. In contrast, the patient already has a certain exercise capacity in the assistive exercise mode, which only needs low auxiliary torque during training. During this process, the robot should provide haptic feedback to induce the patient to complete the training. Therefore, a potential field strategy is used in the assistive exercise mode. In addition, to achieve self-switching between the two modes, a method for assessing the subject’s motor ability is proposed.

The flow chart of dual-modal hybrid self-switching control is shown in Figure 2. It includes mode switching rules, path generator, and position control. Firstly, the sensor data is input to the mode recognition layer after pre-processing. Secondly, the training mode is divided by judging the current motor ability of the patient. Thirdly, the desired exercise trajectory is provided according to the corresponding training mode. Finally, the motor output torque is processed using a smoothing strategy before and after mode switching.

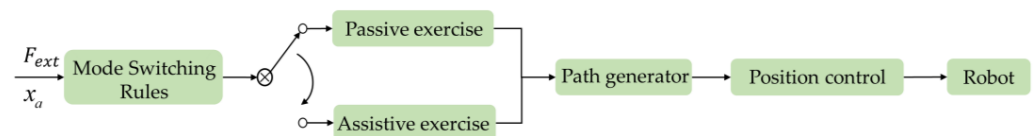


Figure 2. Mode self-switching flow chart.

2.3. Design of Active Disturbance Rejection Position Controller

The position controller of the robot is designed according to the dynamics model of the system. However, the system has high requirements for the design of a position controller, due to the strong nonlinearity of the system itself, coupled with the uncertainty of the model parameters and the external disturbances. The ADRC method can treat the uncertainty terms as an extended state, which can be equivalently compensated in the controller. The ADRC position control block diagram is shown in Figure 3.

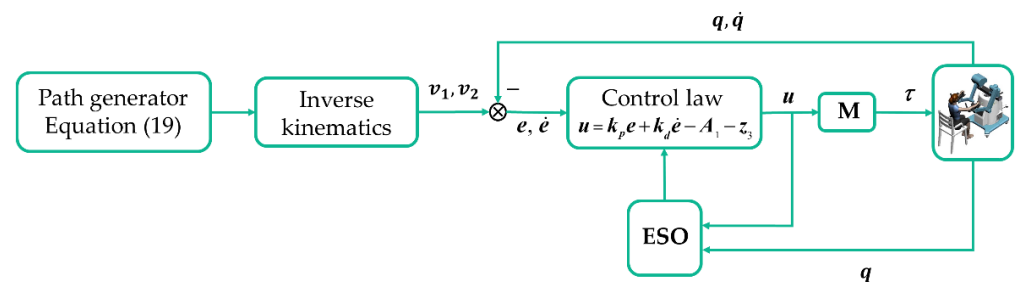


Figure 3. ADRC position control block diagram.

Now assume that $D(t)$ is differentiable. Taking joint 3 as an example, a_{23} is expanded to a new state variable. Let $x_1 = \theta_3$, $x_2 = \dot{\theta}_3$, $\dot{x}_3 = w(t)$, and the state space equation is obtained as follows:

$$\begin{cases} \dot{x}_1 = x_2 \\ \dot{x}_2 = x_3 + a_{13} + u_1 \\ \dot{x}_3 = w(t) \\ y = x_1 \end{cases} \quad (7)$$

The uncertainty term a_{23} is estimated using a third-order extended state observer.

$$\begin{cases} e_1 = z_1 - y \\ \dot{z}_1 = z_2 - \beta_{01}e_1 \\ \dot{z}_2 = z_3 - \beta_{02}e_1 + a_{11} + u_1 \\ \dot{z}_3 = -\beta_{03}e_1 \end{cases} \quad (8)$$

Determining the appropriate observer parameters β_{01} , β_{02} , β_{03} , the system can estimate x_1 , x_2 , x_3 well. x_3 is used as the input of ADRC.

ADRC feedback law is shown:

$$u_1 = k_p e + k_d \dot{e} - a_{11} - z_3 \quad (9)$$

where $e = v_1 - \theta_3$, is the tracking error of joint 3; k_p and k_d denote the proportional and differential coefficients. ADRC position control block diagram is shown in Figure 3.

2.4. Potential Field Design

The potential field is designed based on the desired motion trajectory. The potential energy of the desired trajectory is equal and lowest globally, which means that the potential field gradient is zero at the desired trajectory. The potential energy at each point increases with the distance from the desired trajectory. Deviating from the desired trajectory, the potential field will provide a normal force pointing to the desired trajectory. Therefore, the virtual potential field is designed as follows:

N points are uniformly sampled from the designed trajectory:

$$D_p = \left\{ p_r^i \right\}_{i=1}^N \quad (10)$$

$p_r^i \in R^3$, denotes the position information of the end of the ASM at the i th point in the Cartesian space. D_p denotes discrete desired trajectory dataset of ASM.

$$L_t = \min \left(\left\{ \|p - p_r^i\|_2 \right\}_{i=1}^N \right) \quad (11)$$

L_t is the minimum distance between the point p and each sampling point.

$$\phi^i(p) = \phi_0^i + \frac{1}{2} (p - p_r^i)^T K^i (p - p_r^i) \quad \forall i \in 1 \dots N \quad (12)$$

The virtual energy element $\phi^i(p)$ is established by p and the sampling point p_r^i , ϕ_0^i is a scalar quantity. For a particular point p , there is a virtual spring between p and p_r^i . p is attracted by $-K^i(p - p_r^i)$, and the elastic potential energy of point p is $0.5(p - p_r^i)^T K^i (p - p_r^i)$. It can be seen from Equation (12) that the further the point p is from p_r^i , the higher the elastic potential energy.

Calculate the weight of the potential energy at point p to the N sampling points using the Gaussian kernel function:

$$\omega^i(p) = e^{-\frac{1}{2(\sigma^i)^2} (p - p_r^i)^T (p - p_r^i)} \quad \forall i \in 1 \dots N \quad (13)$$

Normalize the N weights:

$$\tilde{\omega}^i(p) = \frac{\omega^i(p)}{\sum_j \omega^j(p)} \quad \forall i \in 1 \dots N \tag{14}$$

Total potential energy at point p :

$$\Phi(p) = \sum_i \tilde{\omega}^i(p) \phi^i(p) \tag{15}$$

In the potential field, the potential energy is the same at each sampling point. The gradient of the potential field:

$$\nabla \Phi(p) = \sum_i \frac{1}{(\sigma^i)^2} \tilde{\omega}^i(p) (\phi^i(p) - \Phi(p)) (p - p_r^i) - \tilde{\omega}^i(p) K^i (p - p_r^i) \tag{16}$$

On the sampled dataset D_p , The gradient of the designed potential field is expected to be equal to zero. For more details about potential field, please refer to [22]. Therefore, the selection of the potential field parameters ϕ_0^i can be translated into solving the convex optimization problem Equation (17). Finally, using the circle and the straight line segment as the desired trajectory, the designed potential fields are shown in Figure 4.

$$\begin{aligned} \min J(\Theta) &= \frac{1}{N} \sum_{i=1}^N \|\nabla \Phi(p_r^i; \Theta)\|^2 \\ \text{subject to} & \\ 0 \leq \phi_0^i & \quad \forall i = 1 \dots N \\ \nabla \Phi(p_r^i) &= 0 \quad \forall i = 1 \dots N \\ \Theta &= \{\phi_0^1 \dots \phi_0^N\} \end{aligned} \tag{17}$$

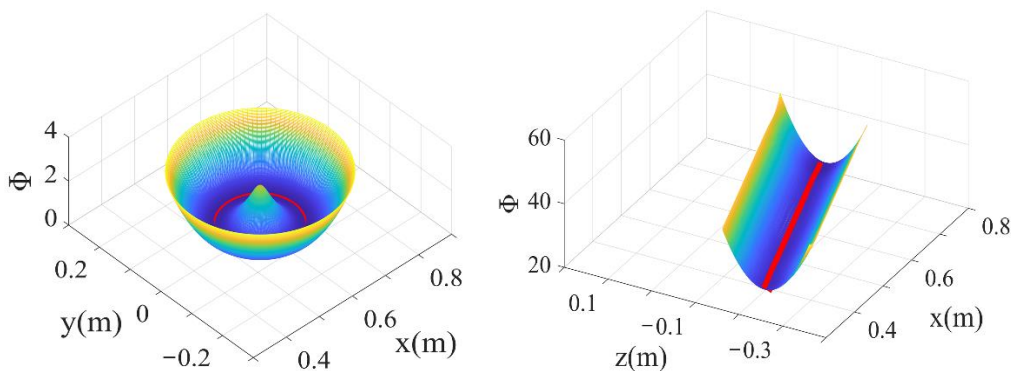


Figure 4. Potential fields generated by two desired trajectories, red line indicates desired trajectory.

2.5. Dual-Modal Hybrid Self-Switching Control

ADRC position controller can precisely track the desired trajectory. By mapping the negative gradient of potential field to the increment of the desired trajectory, potential field can be used for the motion planning of the rehabilitation robot. According to the potential field negative gradient Equation (16), the increment of motion displacement can be obtained as:

$$x_p = -r \nabla \Phi(p) \tag{18}$$

where, r is the coefficient for adjusting the displacement increment, which is positive.

Based on the previously designed ADRC position controller and potential field, the DHSS control strategy is proposed. The control block diagram is shown in Figure 5. The controller consists of two parts, first, passive exercise control: the path generator is used to plan the desired trajectory; second, potential field control: the position of the end of ASM is

found by forward kinematics and the displacement increment for the next control cycle is solved using potential field. Which exercise mode is used depends on the value of α .

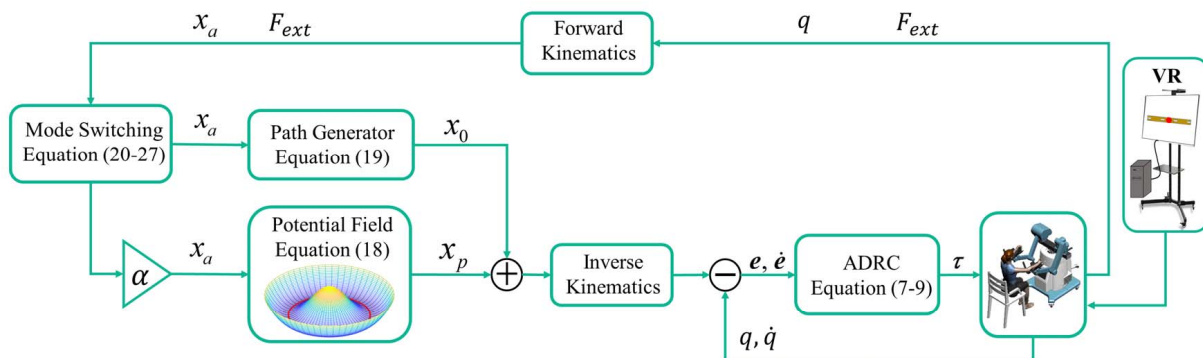


Figure 5. Upper limb rehabilitation robot dual-modal hybrid self-switching control block diagram.

In Figure 5, x_a denotes the actual position of the end of ASM, x_p denotes the displacement increment generated by potential energy field, and x_0 denotes the desired trajectory generated by the path generator. x_0 is as follows:

$$x_0 = \begin{cases} x_t & \alpha = 0 \\ x_a & \alpha = 1 \end{cases} \tag{19}$$

where, x_t represents the desired trajectory in passive exercise mode. The value of α determines the value of x_0 , and the change of the value of α represents the switching of the exercise mode. The self-switching rules of the exercise mode are described in Section 2.6.

2.6. Dual-Modal Self-Switching Rules

To accurately assess patients’ motor ability and to intelligently provide suitable exercise modes, mode self-switching rules are designed in this section. By analyzing the characteristics of the two training modes and the motor ability of the patient during training, effective and generalized evaluation indicators and mode switching thresholds are proposed. It is specified that the initial state of mode is assistive exercise, that assistive exercise to passive exercise is reverse switching, and that passive exercise to assistive exercise is forward switching.

2.6.1. Reverse Switching Rule

Owing to the patient’s muscle strength being insufficient during training, the main exercise method is to rely on the robot to drive the upper limb movement. In reverse switching, the initial state of the robot is assistive exercise mode, which inevitably leads to the inability of patients with severe motor dysfunction to complete the exercise task. To solve this problem, the actual trajectory of ASM is sampled in the period t_1 . If the motion displacement is less than l_0 in the period t_1 , then the exercise mode will be switched to passive exercise. The values of t_1 , l_0 are determined according to the exercise requirements. The specific algorithm is as follows:

End positions of ASM are sampled in time t_1 , and the data set D_x is obtained:

$$D_x = \left\{ p_x^j \in R^3 \right\}_{j=1}^N \tag{20}$$

Find the center position p_0 of D_x :

$$p_0 = \text{mean}(D_x) \tag{21}$$

The sampling point p_{max} in D_x farthest from p_0 :

$$p_{max} = \max \left(\left\{ \|p_x^j - p_0\|_2 \right\}_{j=1}^N \right) \quad (22)$$

Distance between p_0 and p_{max} :

$$l = \text{norm}(p_0 - p_{max}) \quad (23)$$

If l is less than the reverse switching threshold l_0 , the mode is switched to passive exercise. Based on the patient's movement information it is easy to determine the actual movement ability of the patient.

$$\alpha = \begin{cases} 0 & l < l_0 \\ 1 & l \geq l_0 \end{cases} \quad (24)$$

2.6.2. Forward Switching Rule

An impulse is characterized by the cumulative effect of a force acting on an object over some time. Based on the impulse information, the patient's motor intention and motor ability can be detected. The human–robot interaction force can be measured with a force sensor mounted on the end of the ASM. In the passive exercise mode, if patients exert effort in the desired direction of movement during a period of t_2 , then the effective impulse I can be used as an indicator of forward switching.

As shown in Figure 6, taking XY-plane trajectory as an example, the force sensor measures the human–machine interaction force as F_{ext} , the direction of desired motion is v_r , θ is the angle between F_{ext} and v_r , and F is the projection of F_{ext} on v_r . The effective impulse I is the accumulation of F in t_2 time period. I is calculated by the following equation:

$$F = \text{abs} \left(\frac{v_r}{\|v_r\|} \|F_{ext}\| \cos \theta \right) \text{sign}(\cos \theta) \quad (25)$$

$$I = \int_0^{t_2} F dt \quad (26)$$

$$\alpha = \begin{cases} 0 & I < I_0 \\ 1 & I \geq I_0 \end{cases} \quad (27)$$

When θ is an acute angle, it means that the patient's upper limb muscles have done positive work, and F is taken as a positive value at this time. When θ is an obtuse angle, it means that patients have done negative work, and F is taken as a negative value at this time. The value of the period t_2 in Equation (26) is determined by the exercise task. If I is greater than the forward switching threshold I_0 , the mode is turned to assistive exercise. The switching threshold I_0 can be determined through experiments. Assume that the training cycle time is T , the effective impulse is $I_1 = \int_0^T F dt$, and the value range of I_0 : $I_0 \in (0.2I_1, 0.5I_1)$.

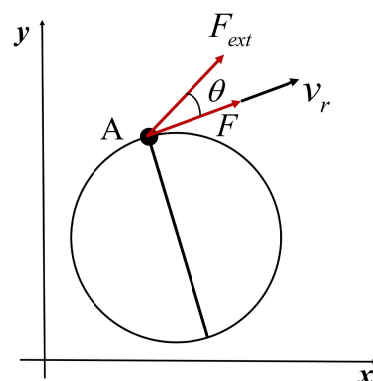


Figure 6. Interaction force F_{ext} and target velocity v_r schematic.

3. Results

In this experiment, the potential field (Figure 4 left) and VR (Figure 7 right) are designed according to the circular trajectory. The center of the circle is (0.6,0,0) m, the radius is 0.1 m, and the circle is located on the XY-plane. The control parameters are $\beta_{01} = 1200$, $\beta_{02} = 4800$, $\beta_{03} = 400$, $k_p = [13 \ 15 \ 15]$, $k_d = [0.7 \ 0.5 \ 0.5]$, $N = 124$, $K = 380 \text{ N/m}$, $\sigma = 0.01$, $r = 1/50$.

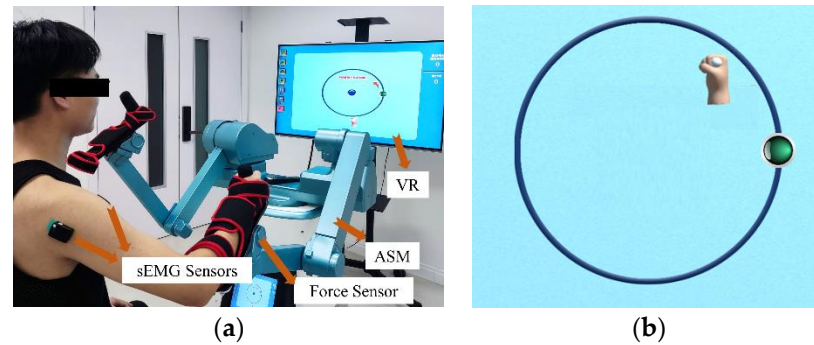


Figure 7. (a) Scene picture of a subject completing rehabilitation task (b) VR.

The experiment was performed by five healthy volunteers (four males and one female, age 21~25 years). All experiments are approved by the Ethics Committee of Cixi Institute of Biomedical Engineering, Ningbo Institute of Materials Technology and Engineering, Chinese Academy of Sciences. All subjects provided informed consent. A passive exercise period of 5 s was set. The scene picture is shown in Figure 7a.

3.1. Experiment on Tracking Error

Subjects simulate passive and assisted exercise of the patient with VR cues. First, the rehabilitation robot enters passive exercise mode under no-load conditions, and the desired trajectory and actual trajectory are recorded for ten cycles. Then, the subjects interact with the ASM to complete the passive exercise for ten cycles. Finally, the exercise mode is switched to assistive exercise for ten cycles. During each task cycle, subjects are asked to maintain consistency in exercise time.

Figure 8 shows the experimental results of one subject: the tracking performance of the three joints of ASM in passive mode, including the actual and desired angles and the tracking error during ten task cycles. It can be seen that the maximum tracking errors of the three joints are 0.28° , 0.5° , and 1° , respectively.

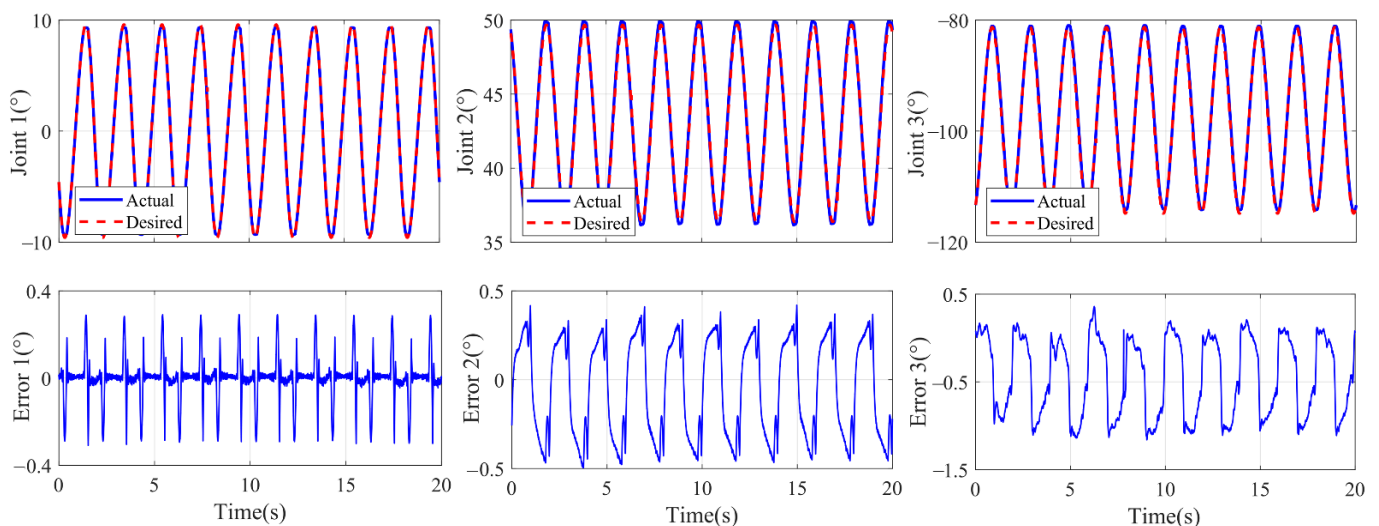


Figure 8. Tracking performance of the three joints of ASM in passive exercise.

Figure 9a shows the actual trajectories in the assistive exercise. It can be seen that the subject can move clockwise in the first 10 s and counterclockwise after 12 s, which proves that the potential field does not compel the subjects to train. Figure 9b shows that the potential field only restricts subjects to exercise around the desired trajectory, which encourages subjects to rely on their own efforts to complete the exercise.

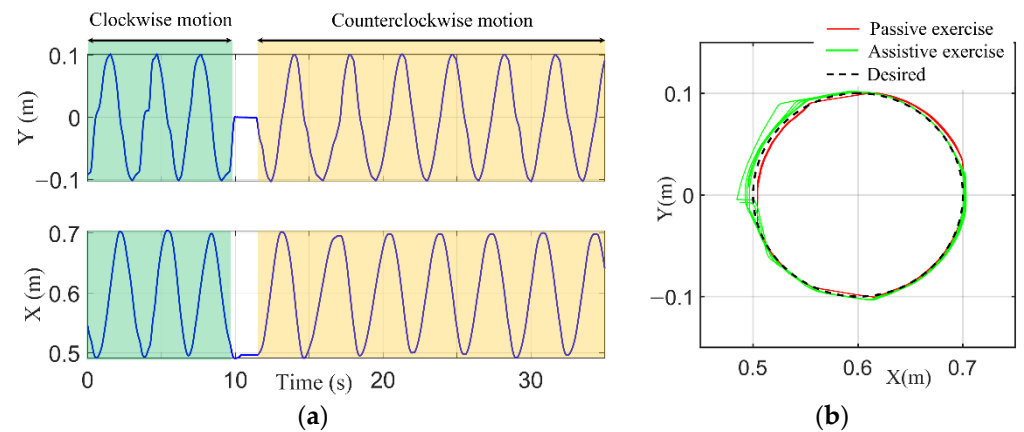


Figure 9. (a) Actual trajectory in assistive exercise. (b) Trajectory in two exercise modes.

The average deviation error L_a and the maximum deviation error L_m in (T_1, T_2) are used to evaluate the effectiveness of the DHSS controller.

$$L_a = \frac{0.001}{T_2 - T_1} \sum_{t=T_1}^{T_2} L_t \quad (28)$$

$$L_m = \max(\{L_t\}_{T_1}^{T_2}) \quad (29)$$

The deviation errors of the five subjects are shown in Table 1. In the passive exercise mode, the maximum deviation error is less than 1 cm, and the average deviation error is less than 1 mm; in the assistive exercise mode, the maximum deviation error is less than 1.03 cm, and the average deviation error is less than 2 mm. The experiment shows that the DHSS controller could assist subjects in completing the exercise with a small level of tracking error in both exercise modes.

Table 1. Subjects' deviation errors in two exercise modes.

Subject	Passive Exercise ($\times 10^{-4}$ m)		Assistive Exercise ($\times 10^{-4}$ m)	
	L_a	L_m	L_a	L_m
no-load	1.88	37	\	\
1	6.14	83	4.28	64
2	9.37	24	7.52	68
3	2.56	40	7.63	88
4	9.61	32	1.40	45
5	2.26	55	16.3	103

3.2. Dual-Modal Self-Switching Experiment

sEMG is a bioelectric signal generated by the contraction of human surface muscles, with voltage amplitude in the range of 0–1.5 mV and frequency concentration in the range of 5–500 Hz. In this paper, the data preprocessing steps of sEMG are as follows: the sEMG is removed mean, band-pass filtered from 5–500 Hz, full-wave rectified, low pass filtered with a cutoff of 1.0 Hz. The processed data is used as eigenvalues of the sEMG [31].

The data collected in this experiment are: the interactive force F_{ext} , the end position of ASM, and the sEMG of the anterior bundle of deltoid muscle (ADM) and the posterior

bundle of deltoid bundle (PDM). The root mean square RMS of the sEMG is used to assess the degree of involvement of the upper limb in the exercise. RMS refers to the magnitude and variability of sEMG over a certain period and is used clinically to describe the number of motor units activated in muscle activity.

$$RMS = \sqrt{\frac{1}{n} \sum_{i=0}^n E_i^2} \tag{30}$$

where n is the number of sEMG data sampled for an exercise task and E_i is the processed sEMG data.

Subjects first complete ten cycles in assistive exercise mode, and then subjects simulate patients with severe motor deficits. The exercise is switched to passive mode because they could not complete the task in time. After completing fifteen cycles of the passive task, subjects gradually exert effort, causing the mode to switch again from passive to assistive. Finally, subjects complete ten cycles of exercise in assistive mode.

Part of the training trajectory of a subject is shown in Figure 10. The red box indicates that the subject has shifted the direction of motion here. As mentioned in Section 2.4, there is no control effect of the potential field during the exercise on the desired trajectory. Therefore, the subject can move clockwise during the first 10 s and counterclockwise from 10–35 s. Around 40 s, the reverse switching rule is triggered because the subject does not continue the movement, and the subject enters passive exercise mode. The variation of the reverse switching parameter l is shown in Figure 11. Note that mode = 1 indicates assistive exercise mode, and mode = 2 indicates passive exercise mode. The reverse switching threshold is $l_0 = 0.05$ m, and the sampling time is: $t_1 = 5$ s. From Figure 11, it can be seen that this subject has been in motion until 40 s, and the l is kept above l_0 . Once l less than l_0 , the robot switches the mode from assistive to passive.

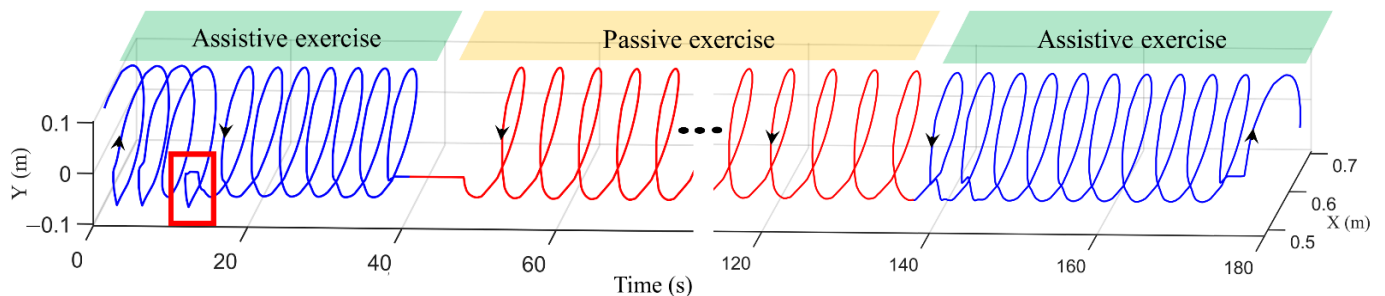


Figure 10. Actual training trajectory.

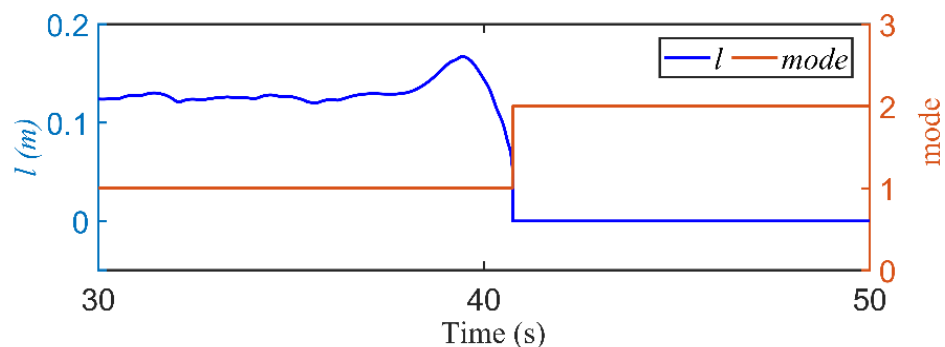


Figure 11. Reverse switching parameter l .

The component of F_{ext} on the X-axis is shown in Figure 12. Around 130 s, this subject starts to actively participate in the training and put more effort, which leads to the triggering of the forward switching rule and the robot switching from the passive mode to the assistive. F_{ext} varies considerably before and after mode switching. Therefore, it makes

sense to use impulse information as a criterion for forward switching. The variation of the forward switching parameter I is shown in Figure 13. The forward switching threshold is set to $I_0 = [8 \ 8 \ -1]$, and the sampling period is $t_2 = 2$ s. Since the desired trajectory is in the XY plane, then the component of I in the Z-axis is 0. From Figure 13, it can be seen that the amplitude of the effective impulse I increases around 130 s. $I > I_0$ at 137 s, the training mode is switched to assistive exercise.

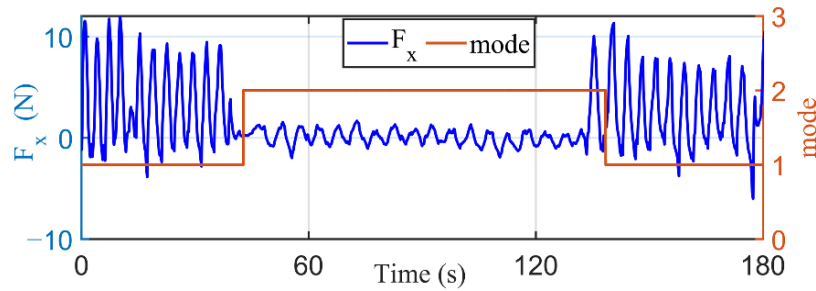


Figure 12. Interaction force and exercise mode.

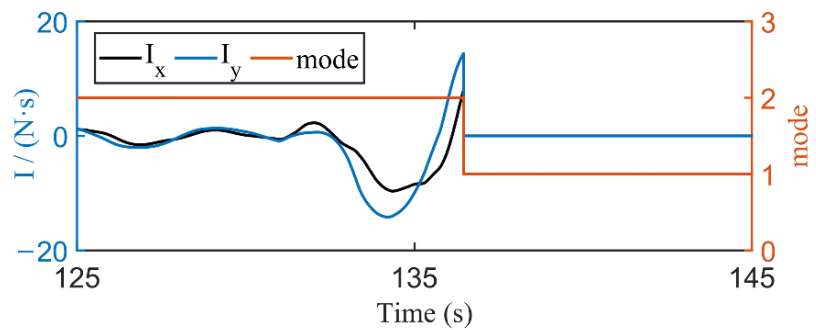


Figure 13. Forward switching parameter I .

The sEMG preprocessing results of ADM and PDM are shown in Figure 14. Subjects have weak motor ability during the passive exercise; the activation of ADM and PDM are low, as is F_{ext} . During the assistive exercise, subjects start to actively participate in the exercise, when the activation of ADM and PDM is high and F_{ext} is at a high level. The results show that the activation levels of ADM and PDM are positively correlated with the training effort of subjects.

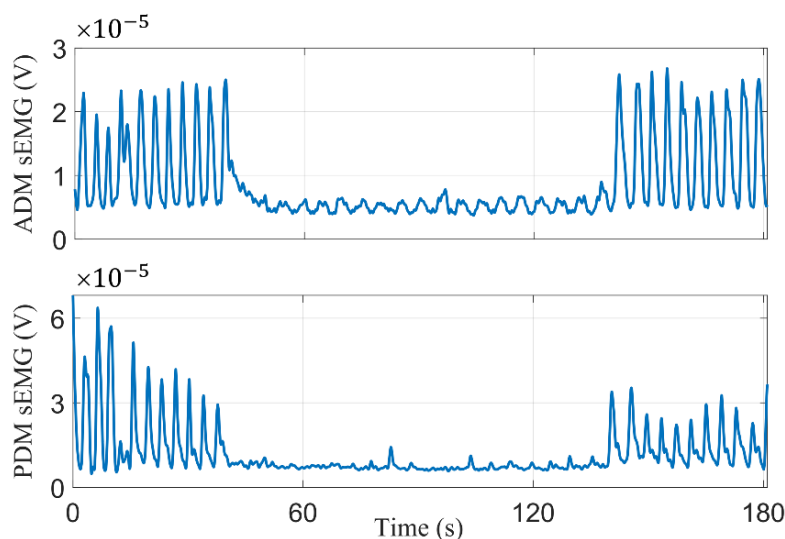


Figure 14. sEMG of ADM and PDM.

Paired samples t-tests are performed for both muscles in both exercise modes, and the results are shown in Table 2 and Figure 15. RMS of sEMG for both muscles in assistive exercise mode is greater than that in the passive exercise mode. RMS of ADM is a significant difference in both modes ($p < 0.05$), and RMS of PDM is a highly significant difference in both modes ($p < 0.005$). Therefore, it can be concluded that the subjects' motor abilities differed significantly before and after mode switching, and that it is reasonable to set thresholds for mode switching.

Table 2. RMS of two muscles in two exercise modes.

Muscle	Assistive Exercise ($\times 10^{-5}$ V)	Passive Exercise ($\times 10^{-5}$ V)	p
ADM	1.941 ± 0.962	1.034 ± 0.509	0.019
PDM	2.914 ± 0.243	0.952 ± 0.374	0.001

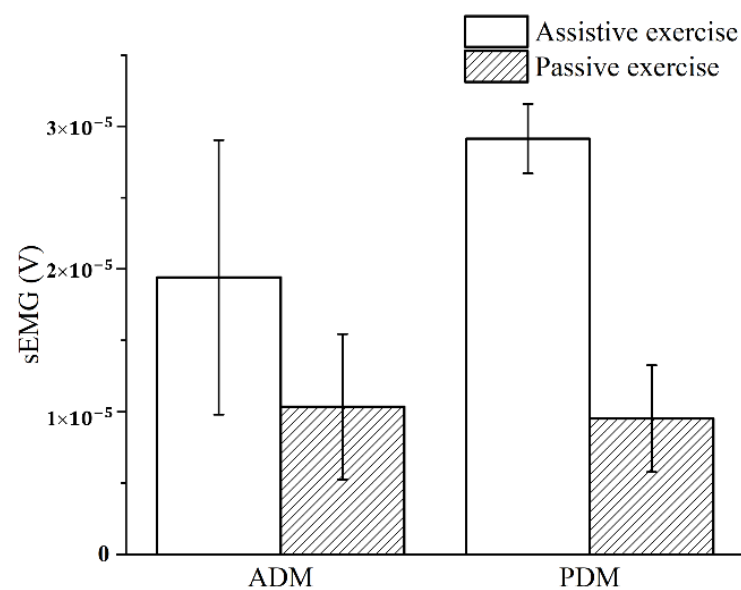


Figure 15. RMS of two muscles in exercise modes.

4. Discussion

Passive exercise is mainly suitable for patients with severe motor deficits. Active participation in training can better promote patients' functional recovery. Therefore, after a large amount of passive exercise, patients' muscle strength performance should be evaluated in time. The assistive exercise mode is selected when the partial motor ability of patients is restored. In addition, considering the cognitive impairment of patients, we used a dual visual and haptic feedback in the task design. Visual feedback was provided by a non-immersive VR, which accurately provides dynamic position information of tasks. Haptic feedback was generated by a designed artificial potential field, which allows patients to perceive the correct training direction.

In this paper, the ADRC method is adopted in the underlying motion controller, while two methods are used for the planning of the desired motion. In passive exercise mode, the path generator can directly generate smooth and stable target trajectories. In the assistive exercise mode, the improved potential field [22,23] is used for path planning considering the compliance of the control strategy. The speed and direction of subjects' motions are entirely determined by themselves, as shown in Figure 10, which also helps to motivate subjects to actively participate in the training. Thus, the potential field is fundamentally different from the time-varying control strategy [18–21]. To evaluate patients' motor ability, dual-modal self-switching rules based on motor and impulse information are proposed. The rationality of the switching indicators is demonstrated with sEMG experiments. This also facilitates the promotion and popularization of the designed rehabilitation robot.

During the rehabilitation of patients with severe motor deficits, the patients were only able to perform passive training due to their lack of muscle strength. According to Figure 14, it can be seen that the sEMG values are low and the muscles are in a state of inactivity when the healthy subjects simulate the patients for passive exercise. However, in the assistive exercise mode, healthy subjects only simulate patients with high motor ability. The level of motor ability of the healthy subjects is not classified, and the subjects only simulate two typical patients with motor dysfunction. Thus, recruitment was limited to only healthy subjects for the experiment in this paper, and patients still need to be recruited. We will further explore the human–robot interaction characteristics of various rehabilitation training modalities in the follow-up [32,33].

According to the training strategy designed in this paper, patients will enter passive exercise mode when they are insufficiently active. This setup will inevitably cause patients to slacken off and rely too much on passive training, rather than stimulating active participation in training. This problem can be addressed by designing attractive VR and introducing reward and punishment mechanisms. In addition, the effects of the proposed training strategies on the rehabilitation training results of patients with motor dysfunction in different age groups have not been investigated. The differences in cognitive, motor and learning abilities of patients at different ages need to be explored in the future, and the control strategy can be further improved.

5. Conclusions

A dual-modal hybrid self-switching control strategy is proposed for the characteristics of human–robot interaction of the upper limb rehabilitation robot. It can be used for self-rehabilitation training of patients with motor dysfunction. The rehabilitation robot provides visual and haptic feedback to patients, which has great potential to improve training accuracy and reduce the difficulty of perceiving training tasks. Dual-modal self-switching rules can accurately determine patients' motor intention, which helps to motivate patients to exercise and improve the rehabilitation effect. The proposed control strategy has significant implications for patient training at home away from the therapist.

Author Contributions: Conceptualization, J.Z. and G.Z.; methodology, G.F.; software, G.F.; validation, G.F. and M.L.; formal analysis, J.Z.; investigation, L.Y.; resources, G.Z. and L.Y.; writing—original draft preparation, G.F. and J.Z.; writing—review and editing, G.F. and D.J.; visualization and supervision, J.Z.; project administration, J.Z. and G.Z.; funding acquisition, G.Z. All authors have read and agreed to the published version of the manuscript.

Funding: This research was supported by the following financial support for the research, authorship, and/or publication of this article: Key Research and Development Program of Zhejiang Province (No.2019C03090); Zhejiang Provincial Natural Science Foundation of China under Grant (No. LGF21H170002); Major Scientific and Technological Projects in Ningbo City (No.2018B10073, 2019B10034, and 2020Z082).

Institutional Review Board Statement: The study was conducted in accordance with the Declaration of Helsinki, and approved by the Ethics Committee of Cixi Institute of Biomedical Engineering, Ningbo Institute of Materials Technology and Engineering, Chinese Academy of Sciences.

Informed Consent Statement: Informed consent was obtained from all subjects involved in the study.

Data Availability Statement: The original data contributions presented in the study are included in the article, further inquiries can be directed to the corresponding authors.

Conflicts of Interest: The authors declare no conflict of interest.

References

1. Everard, G.; Luc, A.; Doumas, I.; Ajana, K.; Stoquart, G.; Edwards, M.G.; Lejeune, T. Self-rehabilitation for post-stroke motor function and activity—A systematic review and meta-analysis. *Neurorehabilit. Neural Repair* **2021**, *35*, 1043–1058. [[CrossRef](#)] [[PubMed](#)]
2. Krebs, H.I.; Hogan, N.; Aisen, M.L.; Aisen, B.T. Robot-aided neurorehabilitation. *IEEE Trans. Rehabil. Eng.* **1998**, *6*, 75–87. [[CrossRef](#)] [[PubMed](#)]

3. Lum, P.S.; Burgar, C.G.; Shor, P.C.; Majmundar, M.; Van der Loos, M. Robot-assisted movement training compared with conventional therapy techniques for the rehabilitation of upper-limb motor function after stroke. *Arch. Phys. Med. Rehab.* **2002**, *83*, 952–959. [[CrossRef](#)] [[PubMed](#)]
4. Zhang, L.; Guo, S.; Sun, Q. Development and assist-as-needed control of an end-effector upper limb rehabilitation robot. *Appl. Sci.* **2020**, *10*, 6684. [[CrossRef](#)]
5. Miao, Q.; Zhang, M.M.; Wang, Y.P.; Xie, S.Q. Design and interaction control of a new bilateral upper-limb rehabilitation device. *J. Healthc. Eng.* **2017**, *2017*, 7640325. [[CrossRef](#)]
6. Nef, T.; Mihelj, M.; Riener, R. ARMin: A robot for patient-cooperative arm therapy. *Med. Biol. Eng. Comput.* **2007**, *45*, 887–900. [[CrossRef](#)]
7. Perry, J.C.; Powell, J.M.; Rosen, J. Isotropy of an upper limb exoskeleton and the kinematics and dynamics of the human arm. *Appl. Bionics Biomech.* **2009**, *6*, 175–191. [[CrossRef](#)]
8. Kim, H.; Miller, L.M.; Fedulow, I.; Simkins, M.; Abrams, G.M.; Byl, N.; Rosen, J. Kinematic data analysis for post-stroke patients following bilateral versus unilateral rehabilitation with an upper limb wearable robotic system. *IEEE Trans. Neural Syst. Rehabil. Eng.* **2013**, *21*, 153–164. [[CrossRef](#)]
9. Perry, J.C.; Rosen, J.; Burns, S. Upper-limb powered exoskeleton design. *IEEE/ASME Trans. Mechatron.* **2007**, *12*, 408–417. [[CrossRef](#)]
10. Wu, Q.; Chen, Y. Development of an intention-based adaptive neural cooperative control strategy for upper-limb robotic rehabilitation. *IEEE Robot. Autom. Lett.* **2021**, *6*, 335–342. [[CrossRef](#)]
11. Chen, C.F.; Du, Z.J.; Zhang, H.; Dong, W. Double-mode switching control of a lower limb exoskeleton based on flexible drive joint. *Jiqiren/Robot.* **2021**, *43*, 513–525.
12. Li, Z.; Zuo, W.K.; Li, S. Zeroing dynamics method for motion control of industrial upper-limb exoskeleton system with minimal potential energy modulation. *Measurement* **2020**, *163*, 107964. [[CrossRef](#)]
13. Reinkensmeyer, D.J.; Dewald, J.P.; Rymer, W.Z. Guidance-based quantification of arm impairment following brain injury: A pilot study. *IEEE Trans. Rehabil. Eng.* **1999**, *7*, 1–11. [[CrossRef](#)] [[PubMed](#)]
14. Horton, S.; Howell, A.; Humby, K.; Ross, A. Engagement and learning: An exploratory study of situated practice in multi-disciplinary stroke rehabilitation. *Disabil. Rehabil.* **2011**, *33*, 270–279. [[CrossRef](#)] [[PubMed](#)]
15. Lenzi, T.; Rossi, S.D.; Vitiello, N.; Carrozza, M.C. Intention-based EMG control for powered exoskeletons. *IEEE Trans. Bio-Med. Eng.* **2012**, *59*, 2180–2190. [[CrossRef](#)] [[PubMed](#)]
16. Benitez, L.; Table, M.; Will, N.; Schmidt, S.; Jordan, M.; Kirchner, E.A. Exoskeleton technology in rehabilitation: Towards an EMG-based orthosis system for upper limb neuromotor rehabilitation. *J. Robot.* **2013**, *2013*, 610589. [[CrossRef](#)]
17. Ho, N.S.K.; Tong, K.Y.; Hu, X.L.; Fung, K.L.; Wei, X.J.; Rong, W.; Susanto, E.A. An EMG-driven exoskeleton hand robotic training device on chronic stroke subjects: Task training system for stroke rehabilitation. In Proceedings of the 2011 IEEE International Conference on Rehabilitation Robotics, Zurich, Switzerland, 29 June–1 July 2011.
18. Sharifi, M.; Behzadipour, S.; Salarieh, H.; Tavakoli, M. Assist-as-needed policy for movement therapy using telerobotics-mediated therapist supervision. *Control. Eng. Pract.* **2020**, *101*, 104481. [[CrossRef](#)]
19. Luo, L.; Peng, L.; Wang, C.; Hou, Z.G. A greedy assist-as-needed controller for upper limb rehabilitation. *IEEE Trans. Neural Netw. Learn. Syst.* **2019**, *30*, 3433–3443. [[CrossRef](#)]
20. Shahbazi, M.; Atashzar, S.F.; Tavakoli, M.; Patel, R.V. Robotics-assisted mirror rehabilitation therapy: A therapist-in-the-loop assist-as-needed architecture. *IEEE/ASME Trans. Mechatron.* **2016**, *21*, 1954–1965. [[CrossRef](#)]
21. Wang, J.; Zhang, J.; Zuo, G.; Shi, C.; Guo, S. A reward-punishment feedback control strategy based on energy information for wrist rehabilitation. *Int. J. Adv. Robot. Syst.* **2020**, *17*, 1729881420940651. [[CrossRef](#)]
22. Khansari-Zadeh, S.M.; Khatib, O. Learning potential functions from human demonstrations with encapsulated dynamic and compliant behaviors. *Auton. Robot.* **2017**, *41*, 45–69. [[CrossRef](#)]
23. Najafi, M.; Rossa, C.; Adams, K.; Tavakoli, M. Using potential field function with a velocity field controller to learn and reproduce the therapist’s assistance in robot-assisted rehabilitation. *IEEE/ASME Trans. Mechatron.* **2020**, *25*, 1622–1633. [[CrossRef](#)]
24. Burns, A.; Adeli, H.; Buford, J.A. Upper limb movement classification via electromyographic signals and an enhanced probabilistic network. *J. Med. Syst.* **2020**, *44*, 176. [[CrossRef](#)]
25. Wang, D.; Zhang, X.; Chen, X.; Zhou, P. Application of wavelet packet transform on myoelectric pattern recognition for upper limb rehabilitation after stroke. In Proceedings of the 2014 36th Annual International Conference of the IEEE Engineering in Medicine and Biology Society, Chicago, IL, USA, 26–30 August 2014.
26. Liparulo, L.; Zhang, Z.; Panella, M.; Gu, X.; Fang, Q. A novel fuzzy approach for automatic Brunnstrom stage classification using surface electromyography. *Med. Biol. Eng. Comput.* **2017**, *55*, 1367–1378. [[CrossRef](#)] [[PubMed](#)]
27. Cai, S.; Chen, Y.; Huang, S.; Wu, Y.; Zheng, H.; Li, X.; Xie, L. SVM-based classification of sEMG signals for upper-limb self-rehabilitation training. *Front. Neurorobot.* **2019**, *13*, 31. [[CrossRef](#)] [[PubMed](#)]
28. Akdoğan, E.; Aktan, M.E.; Koru, A.T.; Arslan, M.S.; Atlıhan, M.; Kuran, B. Hybrid impedance control of a robot manipulator for wrist and forearm rehabilitation: Performance analysis and clinical results. *Mechatronics* **2018**, *49*, 77–91. [[CrossRef](#)]
29. Li, M.; Zhang, J.; Zuo, G.; Feng, G.; Zhang, X. Assist-as-needed control strategy of bilateral upper limb rehabilitation robot based on GMM. *Machines* **2022**, *10*, 76. [[CrossRef](#)]

30. Li, C.B.; Pavelescu, D. The friction-speed relation and its influence on the critical velocity of stick-slip motion. *Wear* **1982**, *82*, 277–289.
31. Potvin, J.R.; Brown, S.H.M. Less is more: High pass filtering, to remove up to 99% of the surface EMG signal power, improves EMG-based biceps brachii muscle force estimates. *J. Electromyogr. Kinesiol.* **2004**, *14*, 389–399. [[CrossRef](#)]
32. Basteris, A.; Nijenhuis, S.M.; Stienen, A.H.; Buurke, J.H.; Prange, G.B.; Amirabdollahian, F. Training modalities in robot-mediated upper limb rehabilitation in stroke: A framework for classification based on a systematic review. *J. Neuro. Eng. Rehabil.* **2014**, *11*, 111. [[CrossRef](#)]
33. Vaida, C.; Carbone, G.; Major, K.A.; Major, Z.Z.; Pisla, D. On human robot interaction modalities in the upper limb rehabilitation after stroke. *Acta Tech. Napoc. Ser. Appl. Math. Eng.* **2017**, *60*, 91–102.